The role of short term memory and conduction velocity restitution in alternans formation

Ning Wei[a], Yoichiro Mori[a], Elena G. Tolkacheva[b,*]

[a]*School of Mathematics, University of Minnesota, Minneapolis, MN 55455*
[b]*Department of Biomedical Engineering, University of Minnesota, Minneapolis, MN 55455*

Abstract

Alternans is the periodic beat-to-beat short-long alternation in action potential duration (APD), which is considered to be a precursor of ventricular arrhythmias and sudden cardiac death. In extended cardiac tissue, electrical alternans can be either spatially concordant (SCA, all cells oscillate in phase) or spatially discordant (SDA, cells in different regions oscillate out of phase). SDA gives rise to an increase in the spatial dispersion of repolarization, which is thought to be proarrhythmic. In this manuscript, we investigated the effect of two aspects of short term memory (STM) (α, τ) and their interplay with conduction velocity (CV) restitution on alternans formation using numerical simulations of a mapping model with two beats of memory. Here, α quantifies the dependence of APD restitution on pacing history and τ characterizes APD accommodation, which is an exponential change of APD over time once basic cycle length (BCL) changes. Our main findings are as follows: In both single cell and spatially coupled homogeneous cable, the interplay between α and τ affects the dynamical behaviors

*Corresponding author
Email address: talkacal@umn.edu (Elena G. Tolkacheva)
[1]Address: 312 Church St. SE, 6-128 Nils Hasselmo Hall, Minneapolis, MN 55455.
[2]Tel.: +1612 626 2719.

of the system. For the case of large APD accommodation ($\tau \geqslant 290$ ms), increase in α leads to suppression of alternans. However, if APD accommodation is small ($\tau \leqslant 250$ ms), increase in α leads to appearance of additional alternans region. On the other hand, the slope of CV restitution does not change the regions of alternans in the cable. However, steep CV restitution leads to more complicated dynamical behaviors of the system. Specifically, SDA instead of SCA are observed. In addition, for steep CV restitution and sufficiently large τ, we observed formations of type II conduction block (CB_2), transition from type I conduction block (CB_1) to CB_2, and unstable nodes.

Keywords: Action potential duration, Mapping model, Single cell, One dimensional cable, Numerical simulation.

---

1. Introduction

Alternans (or so called 2:2 response), a condition in which there is a beat-to-beat alternation in the action potential duration (APD) of a periodically stimulated cardiac cell, has been linked to the genesis of life-threatening ventricular arrhythmias Pastore et al. (1999); Zipes and Wellens (1998); Franz (2003); Myerburg and Spooner (2001). In the heart, alternans can be spatially concordant (SCA) or spatially discordant (SDA). SCA is a phenomenon in which all cells oscillate in phase. SDA is the phenomenon of two spatially distinct regions displaying APD alternans of opposite phases. These regions are separated by nodal lines in which no alternans is present. SDA has recently been related to T wave alternans, a periodic beat-to-beat variation in the amplitude or shape of the T wave in an electrocardiogram Pastore et al. (1999); Zipes and Wellens (1998). T wave alternans is associated with the vulnerability to ventricular arrhythmias and sudden cardiac

death. Therefore, it is accepted that SDA can promote the occurrence of wavebreak and subsequently, reentry Pastore et al. (1999); Pastore and Rosenbaum (2000); Pruvot and Rosenbaum (2003) in the heart, and thus it is proarrhythmic. However, the mechanisms of SDA are not completely understood.

Several mechanisms of SDA formation have been proposed. The first mechanism requires preexisting tissue heterogeneities. SDA can be formed via a timed stimulus or faster pacing rate around regions of heterogeneities Pastore et al. (1999); Chinushi et al. (2003); Pastore et al. (2006). However, as indicated in several numerical studies, tissue heterogeneity is not essential for SDA formation Watanabe et al. (2001); Qu et al. (2000). For example, it has been revealed that SDA can form in a perfectly homogeneous tissue via a pure dynamic mechanism Watanabe et al. (2001). The second proposed mechanism for SDA is a steep dependence of conduction velocity (CV) on the preceding diastolic interval (DI) Franz (2003); Watanabe et al. (2001); Fenton et al. (2002); Fox et al. (2002b); Taggart et al. (2003). A third possible mechanism is unstable intracellular calcium cycling, which refers to the steep relation between calcium release versus sarcoplasmic reticulum calcium load Sato et al. (2013). The last possible mechanism Mironov et al. (2008) is short term memory (STM). The original assumption was that APD depends only on the preceding DI. However, STM implies the dependence of APD on the entire pacing history, not just preceding DI.

The above four mechanisms of SDA formation in cardiac tissue can be distinguished from the behaviors of nodal lines. Nodal lines formed by tissue heterogeneities are displayed by one of the following two scenarios Hayashi et al. (2007). First, once a nodal line forms, it can drift away from the pacing site on a beat-to-beat basis without reaching a steady state. Second, the nodal line may

reach a steady state but remain pinned as pacing rate increases. In contrast, nodal lines formed by steep CV restitution reach steady state and move towards the pacing site at faster pacing rates Hayashi et al. (2007). However, nodal lines formed by unstable calcium cycling are not oriented radially with respect to the pacing site, and also does not move in response to changes in pacing rate Gizzi et al. (2013). On the other hand, it has been suggested that STM is related to unstable behaviors of nodal lines, which means that the nodal lines undergo drifting when pacing rate increases Mironov et al. (2008). However, in experiments, it is difficult to identify the role of each individual mechanism (for example, CV restitution and STM) in alternans formation. In addition, the interplay between these two mechanisms is still unclear.

Therefore, in this manuscript, we aimed to uncover the mechanisms of SDA formation using numerical simulations of a mapping model with two beats of memory that was previously introduced in Tolkacheva et al. (2004). This is a rather simple yet powerful tool to determine the contributions of STM to alternans formation in single cell. In addition, to identify the individual contributions of STM and CV restitution to SDA formation, we will perform numerical simulations of the mapping model in a homogeneous cable.

We adopted the mapping model in the following form Tolkacheva et al. (2004):

$$A_{n+1} = F(D_n,\, A_n,\, D_{n-1}), \tag{1.1}$$

where A_n and D_n are APD and DI at the n^{th} stimulus. Note that, in Eq. (1.1), APD depends not only on the preceding DI, but also on the previous APD and earlier DI, which indicates the presence of two beats of STM in the model. We considered the case of periodic pacing of constant basic cycle length (BCL), for

which relation $A_n + D_n = \text{BCL}$ holds.

2. Materials and Methods

2.1. Mapping model with two beats of memory

For exact form of Eq. (1.1), we used a mapping model that was introduced in Fox et al. (2002a):

$$A_{n+1} = (1 - \alpha M_{n+1}) G(D_n), \tag{2.1a}$$

$$M_{n+1} = [1 - (1 - M_n)\exp(-A_n/\tau)]\exp(-D_n/\tau), \tag{2.1b}$$

where

$$G(D_n) = Q + \frac{R}{1 + \exp(-(D_n - S)/T)}$$

and α and τ are two aspects of STM, which represent rate-dependent restitution and APD accommodation, respectively. Rate-dependent restitution is measured as the difference between slopes of different restitution curves calculated at the same BCL Tolkacheva and Zhao (2012). APD accommodation refers to the slow change of APD over time after an abrupt change in BCL. Note that, large α refers to more disparity between APD restitution curves, and large τ refers to more APD accommodations. We chose the following parameters in Eq. (2.1),

$$Q = 115 \text{ ms},\ R = 121 \text{ ms},\ S = 42.5 \text{ ms},\ T = 20.2 \text{ ms},$$

since these values allowed the mapping model to fit with the steady state solutions from a physiological model of action potential.

In order to investigate the effect of STM on alternans formation using mapping model (2.1), we varied α from 0 to 1 and chose three different values of τ: 11.4 s (large APD accommodation), 260 ms and 200 ms (small APD accommodation).

2.2. Spatially coupled mapping model

In order to model a one dimensional cable, we adopted a spatially coupled mapping model (2.2) by adding diffusion and advection terms to Eq. (1.1), as suggested in Fox et al. (2003):

$$A_{n+1} = F(D_n,\, A_n,\, D_{n-1}) + \xi^2 \nabla^2 A_{n+1} - \omega \nabla A_{n+1}, \tag{2.2}$$

where $\xi = 1, \omega = 0.35$. The choices of ξ and ω were based on Fox et al. (2003); Echebarria and Karma (2007), and detailed justification can be seen in Appendix. Here, the diffusion term $\xi^2 \nabla^2 A_{n+1}$ represents the coupling between cells, and the advection term $-\omega \nabla A_{n+1}$ depicts the asymmetry of influence by its left and right neighbors, considering that cells are activated at different times by the propagating wave front Echebarria and Karma (2002, 2007). The distribution of $D_n(x)$, the n^{th} DI along the cable has been described in Watanabe et al. (2001):

$$\frac{dD_n(x)}{dx} = \frac{1}{V(D_n(x))} - \frac{1}{V(D_{n-1}(x))} - \frac{dA_n(x)}{dx}, \tag{2.3}$$

where x is the position along the cable and V represents a CV restitution curve. Note that, $A_n(0) + D_n(0) = \text{BCL}$. We combined Eq. (2.2) with Eq. (2.3) to solve A_{n+1} along a cable with length $L = 4$ cm, Fox et al. (2003). Due to the finite length of the cable, we imposed the Neumann boundary condition, $\frac{\partial A_{n+1}}{\partial x}|_{x=0,L} = 0$, on the two ends of the cable to minimize the boundary effect. To investigate the effect of CV restitution on SDA formation, we used steep (V_1) and shallow (V_2) restitution curves, as shown in Fig. 1,

$$\begin{aligned} V_1(D_n) &= 0.4 - 0.3\exp(-D_n/10), \\ V_2(D_n) &= 0.4 - 0.03\exp(-D_n/10). \end{aligned} \tag{2.4}$$

We discretized Eqs. (2.2) and (2.3) along a cable with length L by the following scheme at a spatial step size ($\Delta x = \frac{L}{\mathrm{N}}$) of 0.01 cm.

$$-\frac{\xi^2}{\Delta x^2}A_{n+1}(x_{i-1}) + (1+2\frac{\xi^2}{\Delta x^2} - \frac{\omega}{\Delta x})A_{n+1}(x_i) - (\frac{\xi^2}{\Delta x^2} - \frac{\omega}{\Delta x})A_{n+1}(x_{i+1})$$
$$= F(D_n(x_i),\, A_n(x_i),\, D_{n-1}(x_i)),\; i = 1\cdots\mathrm{N},$$

$$A_{n+1}(x_0) = A_{n+1}(x_1),\; A_{n+1}(x_{\mathrm{N}}) = A_{n+1}(x_{\mathrm{N}+1}).$$
$$D_n(x_i) = \mathrm{BCL} + \sum_{j=0}^{i-1}\frac{\Delta x}{V(D_n(x_j))} - \sum_{j=0}^{i-1}\frac{\Delta x}{V(D_{n-1}(x_j))} - A_n(x_i),$$

where x_i is the i^{th} site along the cable, $\Delta x = x_i - x_{i-1}$.

2.3. Pacing protocols

In order to study the mechanism of alternans formation after an abrupt change in pacing rate, BCL was decreased from $\mathrm{BCL}_1 = 500$ ms to a different BCL_2, ranging from 100 ms to 300 ms. We applied 300 stimuli at BCL_1 and sufficient number of stimuli to reach steady state at BCL_2.

In the cable, pacing was applied at the left end $x = 0$, and the following parameters were recorded: steady state positions of nodes (X_{ss}) and time to reach steady state of the nodes (t_{ss}) at BCL_2. Here, X_{ss} was defined as a point for which APD node drifts less than 0.1 mm for the ten consective stimuli. t_{ss} was recorded from the beginning of pacing at BCL_2 until steady state is reached. (See Table 1 for details.)

2.4. Overpacing and conduction block

One of the general limitations of the mapping model is that in a single cell, APD computed using Eq. (2.1) may be larger than $\mathrm{BCL} - D_{\mathrm{min}}$, where $D_{\mathrm{min}} =$ 2 ms is the minimum DI for which an action potential can be initiated Fox et al.

(2002b, 2003); Otani (2007). Slight changes in $D_{\min}$ did not affect our results significantly. If DI $< D_{\min}$, then the cell does not produce an action potential, which will lead to a 2:1 response provided APD $< 2\text{BCL} - D_{\min}$. However, if the cell is further stimulated, it may recover from 2:1 back to 1:1 or 2:2 responses. This phenomenon is known as overpacing, and it is shown in Fig. 2B.

Fig. 2B illustrates responses of mapping model (2.1) when BCL was decreased from BCL_1 to BCL_2. The $(n-1)^{\text{th}}$ and n^{th} stimuli give rise to action potentials, while the $(n+1)^{\text{th}}$ stimulus fails to produce an action potential, since $A_n > A_1^{\text{thr}} = \text{BCL}_2 - D_{\min}$. However, if $A_n < A_2^{\text{thr}} = 2\text{BCL}_2 - D_{\min}$, then the $(n+2)^{\text{th}}$ stimulus will be able to produce an action potential, and

$$\begin{aligned} D_{n+1} &= 2\text{BCL}_2 - A_n, \\ A_{n+2} &= F(D_{n+1}, A_n, D_{n-1}). \end{aligned} \tag{2.5}$$

If a cell can not recover from 2:1 response as a result of overpacing, we defined it as conduction block (CB) for single cell. In general, a $k:1 (k > 2)$ response may be possible if APD $> A_2^{\text{thr}}$.

The effect of overpacing on single cell dynamics for the mapping model (2.1) when BCL was changed from BCL_1 to $\text{BCL}_2 = 170$ ms is demonstrated in Fig. 3. It shows an example of CB (A) and transition from 2:1 to 1:1 responses (B) as a result of overpacing. Here, $\alpha = 0.1$ (A), $\alpha = 0.6$ (B) and $\tau = 11.4$ s. As observed in Fig. 3A, APDs (open circles) are always greater than A_1^{thr} (dashed line) but less than A_2^{thr} (dashed line), indicating a sustained 2:1 response.

In contrast, in Fig. 3B, APDs are greater than A_1^{thr} and less than A_2^{thr} at the beginning of pacing at BCL_2. But with continued pacing, APD becomes less than A_1^{thr}, thus indicating the transition from 2:1 response to 1:1 behavior can only be observed in the presence of overpacing.

In a cable, one may have $D_n(x) \geqslant D_{\min}$ for certain x, whereas $D_n(x) < D_{\min}$ for other x. Several scenarios of dealing with CB and overpacing in the cable have been discussed in the literature. For example, in Otani (2007), the authors developed a method that uses the APD and CV restitution relations to generate predictions regarding which sequences of premature stimuli are most likely to induce type II CB and reentry. Specifically, block occurs when the trailing edge of the preceding wave travels slower than the leading edge of the current wave, allowing the latter to encroach and terminate on the former. In Fox et al. (2003), simulation was terminated once $D_n(x) < D_{\min}$ occurred for any x in the cable. In Fox et al. (2002b), overpacing was considered for a cable consisting of a simple mapping model without memory, $A_{n+1} = f(D_n)$.

In this manuscript, we implemented overpacing in the cable for the mapping model with two beats of STM by using the approach shown in Fig. 2C, which illustrates responses of spatially coupled mapping model (2.2) when the cable was paced at $x = 0$ and BCL was decreased from BCL_1 to BCL_2. As observed, solid and dashed lines represent the wavefront and waveback of an action potential along the cable, respectively. Let x^* be the maximal value such that

$$\widetilde{D_n(x)} \geqslant D_{\min}, \text{ for } x < x^*, \tag{2.6}$$

where $\widetilde{D_n(x)}$ satisfies the following:

$$\frac{d\widetilde{D_n(x)}}{dx} = \frac{1}{V(\widetilde{D_n(x)})} - \frac{1}{V(D_{n-1}(x))} - \frac{dA_n(x)}{dx},$$

$$A_n(0) + \widetilde{D_n(0)} = \mathrm{BCL}.$$

Then we let $D_n(x) = \widetilde{D_n(x)}$ for $x < x^*$, where $D_n(x)$ is the n^{th} DI. That is, the $(n+1)^{\text{th}}$ action potential can only propagate to x^*. Therefore, $A_{n+1}(x)$ also exists

for $x < x^*$ (we let $A_{n+1} = 0$ for $x \geqslant x^*$ to emphasize).

Let us consider the situation when the $(n+2)^{\text{th}}$ action potential can propagate to the end. For $x < x^*$, $D_{n+1}(x)$ and $A_{n+2}(x)$ can be obtained by Eqs. (2.2) and (2.3). For $x \geqslant x^*$, $D_{n+1}(x)$ and $A_{n+2}(x)$ can be obtained by Eq. (2.7) below.

$$\begin{aligned} \frac{dD_{n+1}(x)}{dx} &= \frac{1}{V(D_{n+1}(x))} - \frac{1}{V(D_{n-1}(x))} - \frac{dA_n(x)}{dx}, \\ A_{n+2} &= F(D_{n+1},\, A_n,\, D_{n-1}) + \xi^2 \nabla^2 A_{n+2} - \omega \nabla A_{n+2}, \end{aligned} \tag{2.7}$$

where $D_{n+1}(x)$ is the DI that follows either $A_{n+1}(x)$ (for $x < x^*$) or $A_n(x)$ (for $x \geqslant x^*$). If the action potential can not propagate to the end of the cable, CB occurs. Moreover, if CB occurs at $x = 0$, we defined it as type I CB (CB_1). If CB occurs at $x \neq 0$, we defined it as type II CB (CB_2).

3. Results

3.1. Dynamical responses of single cell

We first aimed to classify different dynamical behaviors of the mapping model (2.1) at steady state (i.e. 1:1, 2:2, or CB) when BCL was changed from BCL_1 to various BCL_2. Fig. 4 illustrates steady state responses at different BCL_2 as a function of α for $\tau = 11.4$ s (A), $\tau = 260$ ms (B), and $\tau = 200$ ms (C). Black dashed lines outline the regions for 1:1 responses (filled circles or upper right corner regions labeled as 1:1) and CB. For $\tau = 11.4$ s and 260 ms (Figs. 4A and 4B), we can see that when BCL_2 is large, only 1:1 responses are observed. As BCL_2 decreases, CB or 2:2 (or alternans) (crosses) behaviors occur, which transition to 1:1 responses as α increases. Once BCL_2 becomes sufficiently small, only CB is observed.

Fig. 4C shows different dynamical responses of the mapping model (2.1) for $\tau = 200$ ms. Here, we can see a larger region occupied by alternans (crosses), especially for large α. These results suggest that the effect of α is diminished as τ decreases.

The dynamical behaviors of a single cell are different for high and low values of τ. The cases $\tau = 11.4$ s and $\tau = 200$ ms are two representatives of the respective regimes. The high τ regime extends to about 290 ms and the low τ regime extends to around 250 ms. There is a narrow transition regime between $\tau = 250$ ms and $\tau = 290$ ms, for which we showed the case $\tau = 260$ ms.

The individual roles of α and τ in alternans formation can be understood by considering the limit of M_{n+1} as τ approaches zero. Eq. (2.1b) yields $\lim_{\tau\to 0} M_{n+1} = \lim_{\tau\to 0}[1-(1-M_n)\exp(-A_n/\tau)]\exp(-D_n/\tau) = 0$, since A_n, $D_n > 0$. Then Eq. (2.1a) reduces to $A_{n+1} = G(D_n)$, i.e. no memory. Thus, effect of α is diminished as τ decreases.

3.2. SDA in spatially coupled mapping model

3.2.1. Effect of overpacing on CB

We found that the effect of overpacing has more important consequences on dynamics in the cable, in comparison to the single cell. To illustrate it, we performed numerical simulations of spatially coupled mapping model (2.2) when BCL was decreased from BCL_1 to BCL_2. Figs. 5A – 5E show results for different stimulus number at $\mathrm{BCL}_2 = 220$ ms, $\alpha = 0.175$, $\tau = 11.4$ s and $\mathrm{CV} = V_1$. As observed, Fig. 5A demonstrates that CB_1 occurred at the first beat as BCL was decreased to BCL_2, after which SCA (Fig. 5B) and SDA (Figs. 5C and 5D) occurred sequentially. SDA persists for about 40 beats, and then CB_2 (Fig. 5E) is observed at the 59^{th} beat, at which action potential is blocked in the middle of the

cable.

In Fig. 5F, we set $\mathrm{BCL}_2 = 190$ ms, $\alpha = 0.425$, $\tau = 11.4$ s and $\mathrm{CV} = V_1$. As stimuli number increases, we observed a transition from CB_1 (dashed line) to SDA (open and filled circles) and then to 1:1 (grey line) behavior under overpacing. Note that, neither the transition from CB_1 to CB_2 nor the transition from CB_1 to SDA and then to 1:1 response can be observed without overpacing. Instead, simulations would have terminated at the first beat.

3.2.2. SDA node behaviors while approaching steady state

We observed two different behaviors of SDA nodes while approaching steady state: stable and unstable node formation. Fig. 6A shows stable behavior of nodes for the spatially coupled mapping model (2.2) when BCL was decreased from BCL_1 to $\mathrm{BCL}_2 = 240$ ms, $\alpha = 0.175$, $\tau = 11.4$ s and $\mathrm{CV} = V_1$. Note that the node formed by the 188^{th} and 189^{th} beats (black dashed) appears at the distal end of the cable and then moves towards (grey and black nodes) the pacing site $x = 0$ as it approaches steady state X_{ss}.

Fig. 6B shows unstable behavior of the node for the spatially coupled mapping model (2.2) when BCL was decreased from BCL_1 to $\mathrm{BCL}_2 = 210$ ms, $\alpha = 0.3$, $\tau = 11.4$ s and $\mathrm{CV} = V_1$. The node formed by the 6^{th} and 7^{th} beats (black dashed) appears at the end of the cable and migrates towards (grey solid) the pacing site $x = 0$ first, and then away from (black solid) the pacing site $x = 0$ as it approaches steady state X_{ss}.

For the stable nodes, we calculated the steady state positions (X_{ss}) and time to reach steady state (t_{ss}). Figs. 7A and 7B are representative examples displaying X_{ss} and t_{ss} as a function of α respectively. Both figures were obtained for the spatially coupled mapping model (2.2) when BCL was changed from BCL_1 to

$BCL_2 = 130$ms, where $\tau = 200$ ms and CV $= V_1$. As depicted, X_{ss} increases as α increases and t_{ss} first decreases and then increases. Our results show that increase of α could result in steady state nodes being further away from pacing site. Nevertheless, there appears to be a minimum t_{ss} as α is varied in Fig. 7B.

3.2.3. Interplay between CV restitution and STM

Finally, we aimed to characterize different dynamical behaviors of the spatially coupled mapping model (2.2) at steady state when BCL was changed from BCL_1 to various BCL_2. Fig. 8 illustrates steady state responses at different BCL_2 as a function of α for V_2 (shallow CV restitution), $\tau = 11.4$ s (A), $\tau = 260$ ms (B), $\tau = 200$ ms (C) and for V_1 (steep CV restitution), $\tau = 11.4$ s (D), $\tau = 260$ ms (E), $\tau = 200$ ms (F). As observed in Figs. 8A – 8C, at CV $= V_2$, steady state behaviors in the cable looked very similar to those of single cell if SDA (cross) and SCA (square) are considered as alternans, since single cells cannot exhibit spatial phenomena.

Figs. 8A and 8D illustrate that for $\tau = 11.4$ s, steep CV restitution (V_1, Fig. 8D) leads to appearance of more complicated dynamical responses, such as CB_2 (diamond) (Fig. 5E), transition from CB_1 to CB_2 (star, $CB_1 \rightarrow CB_2$) (Figs. 5A – 5E) and unstable nodes (plus, unstable) (Fig. 6B).

However, Figs. 8B, 8C, 8E, 8F illustrate that for $\tau = 260$ ms and 200 ms, the effect of steep CV restitution curves is negligible, except more formation of SDA, including the region of large α.

Furthermore, Figs. 8D and 8F illustrate that for V_1, smaller τ (200 ms) leads to appearance of simpler dynamical responses, such as the inhibition of CB_2 (diamond), transition from CB_1 to CB_2 (star, $CB_1 \rightarrow CB_2$), and unstable nodes (plus, unstable).

Similar to the single cell case, the dynamical behaviors of the cable are different for high and low values of τ. The cases $\tau = 11.4$ s and $\tau = 200$ ms are two representatives of the respective regimes. We also showed results for $\tau = 260$ ms, at which the behavior is intermediate between the two regimes.

Our results indicate that shallow CV restitution together with large τ can help suppress SDA. Steep CV restitution coupled with large τ gives rise to CB_2, the transition from CB_1 to CB_2 and unstable nodes, which are inhibited by either shallow CV or small τ. Steep CV restitution together with small τ can lead to more formation of SDA, including the region of large α. Our result also indicates that STM plays a dominant role in SDA formation.

4. Conclusion and Discussion

In this manuscript, we investigated the effect of two aspects of STM (α, τ) and their interplay with CV restitution on alternans formation using numerical simulations of a mapping model with two beats of memory. In both single cell and spatially coupled homogeneous cable, the interplay between α and τ affects the dynamical behaviors of the system. For the case of large APD accommodation ($\tau \geqslant 290$ ms), an increase in α leads to suppression of alternans. However, if APD accommodation is small ($\tau \leqslant 250$ ms), an increase in α leads to appearance of additional alternans region. On the other hand, the slope of CV restitution does not change the regions of alternans in the cable. However, steep CV restitution leads to more complicated dynamical behaviors of the system. Specifically, SDA instead of SCA are observed. In addition, for steep CV restitution and sufficiently large τ, we observed formations of CB_2, transition from CB_1 to CB_2, and unstable nodes.

To our knowledge, this is the first use of overpacing in a mapping model with two beats of memory. At the single cell level, the cell may recover from 2:1 rhythm back to 1:1 or 2:2 rhythm if the cell is stimulated beyond the beat at which $\mathrm{DI} < D_{\min}$. The same can be said of the cable. This indicates the importance of pacing beyond conduction block. In Fox et al. (2003), stimulation was terminated once $\mathrm{DI}(x) < D_{\min}$ for any x in the cable. In Fox et al. (2002b), overpacing was adopted using a simple mapping model without memory; APD only depended on the preceding DI, making it relatively simple to implement overpacing. Here, we overpaced the cable in a mapping model with two beats of memory. The dependence of APD on the preceding APD and two preceding DIs gives rise to new difficulties in the continuation of pacing after $\mathrm{DI} < D_{\min}$ for any x in the cable. The resolution of this difficulty is a technical contribution of our paper. Our use of continued pacing has allowed us to observe recoveries from CB_1 to 1:1 responses or SDA and transitions from CB_1 to CB_2 that we would not have been able to see otherwise.

This is the first study in which a mapping model with two beats of memory has been used to investigate SDA formation. Over the last decades, the study of SDA has become a major focus of research because of its potentially crucial link to cardiac instability. Our numerical results are in agreement with previous experimental and theoretical studies of SDA. We confirmed that SDA can be observed in a homogeneous cable Watanabe et al. (2001); Qu et al. (2000), and that steep CV restitution facilitates SDA Franz (2003); Watanabe et al. (2001); Fenton et al. (2002); Fox et al. (2002b); Taggart et al. (2003). We also found that small τ, together with steep CV restitution, further facilitates SDA formation. This agrees with the experimental results in Mironov et al. (2008) which states that stable

SDA nodal lines were associated with steep CV restitution and small τ. Finally, we demonstrated that unstable behaviors of nodes is related to steep CV restitution and large τ. This is consistent with experimental results in Mironov et al. (2008), wherein the unstable drifting behaviors of nodal lines during adaptation to change in BCL are seen for large values of τ.

One limitation of our study is that we chose $D_{\min} = 2$ ms. However, our simulation results demonstrate that sufficiently large increases in $D_{\min}$ might affect the dynamic behaviors of the cable model. Specifically, for $D_{\min} = 20$ ms, $\tau = 11.4$ s and CV $= V_1$ (steep CV restitution), we observed more incidences of CB_1 as well as transitions from SCA or SDA to CB_2, the latter of which were not present for $D_{\min} = 2$ ms.

Another limitation of our study is that we chose the cable length L to be 4 cm with 401 cells. It is clear that we will see more incidences of SDA and nodes in a larger domain. However, if simulations are performed on a larger domain with length $L > 4$ cm, but the dynamical behaviors are only tracked on the first 4 cm segment of the simulation domain, we have checked that the simulation results are similar to the case when $L = 4$ cm. This indicates that the boundary conditions at $x = L$ do not appreciably affect the results of the simulation.

5. Appendix: Derivation of ξ and ω.

Numerical solutions to Eq. (2.1) together with Eq. (2.3) develops unphysical spatial discontinuities along the cable, as observed in Echebarria and Karma (2002). This can be avoided by considering the cell coupling effect, which contributes diffusion and advection terms, as has been suggested in Echebarria and Karma (2002, 2007). Therefore, in order to model a one dimensional cable, we

adopted a spatially coupled mapping model (2.2) by adding diffusion and advection terms to Eq. (1.1), as suggested in Fox et al. (2003).

Here, we discuss the values for ξ and ω that were used in Eq. (2.2) following Fox et al. (2003). An interpretation of ξ and ω can be found in Echebarria and Karma (2007). The starting point is the following equation:

$$\mathrm{A}_{n+1}(x) = (G * f)(x) = \int_{-\infty}^{+\infty} G(y) f[\mathrm{D}_n(x-y)]dy. \tag{5.1}$$

where $G(y)$ is some normalized asymmetrical kernel that expresses the diffusive coupling between neighboring cells. Let us define the Fourier transform $(\mathscr{F}(\cdot))$ of the kernel to be $(\mathscr{F}(G))(k) = \int_{-\infty}^{+\infty} G(y)e^{-iky}dy$. The exponential function in the above equation can be expanded in the form $e^{-iky} = 1 - iky - (ky)^2/2 + \cdots$. It then follows that

$$(\mathscr{F}(G))(k) = 1 - i\widehat{\omega}k - \widehat{\xi}^2 k^2 + \cdots, \tag{5.2}$$

where the coefficients are defined as

$$\widehat{\omega} = \int_{-\infty}^{+\infty} G(y)ydy, \;\; \widehat{\xi}^2 = \frac{1}{2}\int_{-\infty}^{+\infty} G(y)y^2dy.$$

Now, consider the equation

$$(I - \xi^2\nabla^2 + \omega\nabla)A_{n+1} = f(D_n). \tag{5.3}$$

This is the same as Eq. (2.2) except that the mapping model f only depends on D_n. Let us relate ξ and ω above with $\widehat{\xi}$ and $\widehat{\omega}$ of Eq. (5.2). By taking Fourier transform of both sides, we have

$$\mathscr{F}(A_{n+1}) = \frac{1}{1 + i\omega k + \xi^2 k^2}\mathscr{F}(f). \tag{5.4}$$

Therefore,

$$A_{n+1}(x) = (G * f)(x), \text{ where } (\mathscr{F}(G))(k) = \frac{1}{1 + i\omega k + \xi^2 k^2}. \tag{5.5}$$

By Taylor expansion, we see that

$$(\mathscr{F}(G))(k) = 1 - i\omega k - (\xi^2 + \omega^2)k^2 + \cdots .$$

Comparing the above with Eq. (5.2), we have

$$\widehat{\omega} = \omega, \ \widehat{\xi}^2 = \xi^2 + \omega^2.$$

If $\omega^2 \ll \xi^2$, then $\widehat{\xi}^2 = \xi^2$. Therefore, $G = \mathscr{F}^{-1}(\frac{1}{1+i\omega k+\xi^2 k^2})$. We point out that Eq. (5.1) (or a discretized version thereof) has been used in several other publications to describe electronic couplings between cells. For example, the papers Fox et al. (2002b) and Vinet (2000) used the Gaussian kernel $G(y) = \exp(-\mu y^2)$.

Note that Eq. (5.1) is an approximation. It is more realistic to use a biophysical ionic model, and it is thus of interest to relate Eq. (5.1) to ionic models. For a simple two variable ionic model, Echebarria and Karma (2007) demonstrated that $\widehat{\omega}$ and $\widehat{\xi}$ can be calculated explicitly in certain limiting cases, giving

$$\widehat{\omega} = \frac{2D}{c}, \quad \widehat{\xi} = (D \times \mathrm{APD}_c)^{1/2},$$

where D denotes the diffusion coefficient in the two variable ionic model, c denotes CV of a propagating wave and APD_c denotes APD at the bifurcation point. Using typical values of D, c and APD_c, the length $\widehat{\xi}$ is on the order of 1 mm, while $\widehat{\omega}$ is on the order 0.1 mm.

The authors of Fox et al. (2003) adjusted the value of $\omega(=\widehat{\omega})$ to 0.35 mm in order to produce spatial patterns that were similar to what they observed experimentally. We also investigated the effect of changing ω on dynamic behaviors of spatially coupled mapping model, and determined that it has a minor effect. For instance, $\omega = 0.1$ mm leads to simpler dynamic behaviors. Therefore, we used $\xi = 1$ mm and $\omega = 0.35$ mm in our manuscript, without loss of generality.

6. Acknowledgement

This work was supported by National Science Foundation grants CMMI-1233951 and NSF CAREER PHY-125541 to E.G.T. Y.M. was supported by NSF grant DMS 0914963, the Alfred P. Sloan Foundation and the McKnight Foundation. In addition, we would like to thank all the referees for careful reading of the paper and valuable suggestions.

7. References

Chinushi, M., Kozhevnikov, D., Caref, E. B., Restivo, M., El-Sherif, N., 2003. Mechanism of discordant t wave alternans in the in vivo heart. J. Cardiovasc. Electrophysiol. 14 (6), 632–638.

Echebarria, B., Karma, A., 2002. Instability and spatiotemporal dynamics of alternans in paced cardiac tissue. Phys. Rev. Lett. 88 (20), 208101.

Echebarria, B., Karma, A., 2007. Amplitude equation approach to spatiotemporal dynamics of cardiac alternans. Phys. Rev. E 76 (5), 051911.

Fenton, F. H., Cherry, E. M., Hastings, H. M., Evans, S. J., 2002. Multiple mechanisms of spiral wave breakup in a model of cardiac electrical activity. Chaos 12 (3), 852–892.

Fox, J. J., Bodenschatz, E., Gilmour Jr, R. F., 2002a. Period-doubling instability and memory in cardiac tissue. Phys. Rev. Lett. 89 (13), 138101.

Fox, J. J., Riccio, M. L., Drury, P., Werthman, A., Gilmour Jr, R. F., 2003. Dynamic mechanism for conduction block in heart tissue. New J. Phys. 5 (1), 101–114.

Fox, J. J., Riccio, M. L., Hua, F., Bodenschatz, E., Gilmour, R. F., 2002b. Spatiotemporal transition to conduction block in canine ventricle. Circ. Res. 90 (3), 289–296.

Franz, M. R., 2003. The electrical restitution curve revisited: steep or flat slope–which is better? J. Cardiovasc. Electrophysiol. 14 (s10), S140–S147.

371 Gizzi, A., Cherry, E. M., Gilmour Jr, R. F., Luther, S., Filippi, S., Fenton, F. H.,
372 2013. Effects of pacing site and stimulation history on alternans dynamics and
373 the development of complex spatiotemporal patterns in cardiac tissue. Front.
374 Physiol. 4, 71.

375 Hayashi, H., Shiferaw, Y., Sato, D., Nihei, M., Lin, S.-F., Chen, P.-S., Garfinkel,
376 A., Weiss, J. N., Qu, Z., 2007. Dynamic origin of spatially discordant alternans
377 in cardiac tissue. Biophys. J. 92 (2), 448–460.

378 Mironov, S., Jalife, J., Tolkacheva, E. G., 2008. Role of conduction velocity resti-
379 tution and short-term memory in the development of action potential duration
380 alternans in isolated rabbit hearts. Circulation 118 (1), 17–25.

381 Myerburg, R. J., Spooner, P. M., 2001. Opportunities for sudden death prevention:
382 directions for new clinical and basic research. Cardiovasc. Res. 50 (2), 177–185.

383 Otani, N. F., 2007. Theory of action potential wave block at-a-distance in the
384 heart. Phys. Rev. E 75 (2), 021910.

385 Pastore, J. M., Girouard, S. D., Laurita, K. R., Akar, F. G., Rosenbaum, D. S.,
386 1999. Mechanism linking t-wave alternans to the genesis of cardiac fibrillation.
387 Circulation 99 (10), 1385–1394.

388 Pastore, J. M., Laurita, K. R., Rosenbaum, D. S., 2006. Importance of spatiotem-
389 poral heterogeneity of cellular restitution in mechanism of arrhythmogenic dis-
390 cordant alternans. Heart Rhythm 3 (6), 711–719.

391 Pastore, J. M., Rosenbaum, D. S., 2000. Role of structural barriers in the mecha-
392 nism of alternans-induced reentry. Circ. Res. 87 (12), 1157–1163.

Pruvot, E. J., Rosenbaum, D. S., 2003. T-wave alternans for risk stratification and prevention of sudden cardiac death. Curr. Cardiol. Rep. 5 (5), 350–357.

Qu, Z., Garfinkel, A., Chen, P.-S., Weiss, J. N., 2000. Mechanisms of discordant alternans and induction of reentry in simulated cardiac tissue. Circulation 102 (14), 1664–1670.

Sato, D., Bers, D. M., Shiferaw, Y., 2013. Formation of spatially discordant alternans due to fluctuations and diffusion of calcium. PlOS ONE 8 (12), e85365.

Taggart, P., Sutton, P., Chalabi, Z., Boyett, M. R., Simon, R., Elliott, D., Gill, J. S., 2003. Effect of adrenergic stimulation on action potential duration restitution in humans. Circulation 107 (2), 285–289.

Tolkacheva, E. G., Romeo, M. M., Guerraty, M., Gauthier, D. J., 2004. Condition for alternans and its control in a two-dimensional mapping model of paced cardiac dynamics. Phys. Rev. E 69 (3), 031904.

Tolkacheva, E. G., Zhao, X., 2012. Nonlinear dynamics of periodically paced cardiac tissue. Nonlinear Dyn. 68 (3), 347–363.

Vinet, A., 2000. Quasiperiodic circus movement in a loop model of cardiac tissue: Multistability and low dimensional equivalence. Annals of biomedical engineering 28 (7), 704–720.

Watanabe, M. A., Fenton, F. H., Evans, S. J., Hastings, H. M., Karma, A., 2001. Mechanisms for discordant alternans. J. Cardiovasc. Electrophysiol. 12 (2), 196–206.

414 Zipes, D. P., Wellens, H. J., 1998. Sudden cardiac death. Circulation 98 (21),
415 2334–2351.

8. Figure Captions

Fig. 1 : CV as a function of D_n, for steep restitution curves V_1 (solid) and shallow V_2 (dashed).

Fig. 2 : Periodic pacing of single cell leading to 1:1 responses (A). Overpacing of single cell (B) and cable (C). In A, action potentials occur as a result of periodic stimulation, i.e., $A_n + D_n = \mathrm{BCL}$. In B, action potentials are shown for pacing protocol in which BCL was changed from BCL_1 to BCL_2. Note that, $(n-1)^{\mathrm{th}}$ and n^{th} stimuli produce action potentials, but the $(n+1)^{\mathrm{th}}$ stimulus (dashed vertical line) fails to produce an action potential. However, if the $(n+2)^{\mathrm{th}}$ beat produces an action potential, then D_{n+1} and A_{n+2} can be obtained by Eq. (2.5). In C, solid and dashed lines represent the wavefront and waveback of an action potential, respectively. The $(n-1)^{\mathrm{th}}$ and n^{th} stimuli produce action potentials that propagate to the end of the cable. But the $(n+1)^{\mathrm{th}}$ action potential can only be delivered for $x < x^*$, i.e. CB occurs at $x = x^*$. Note that, the $(n+2)^{\mathrm{th}}$ action potential can propagate to the end of the cable.

Fig. 3 : CB (A) and overpacing leading to transition from 2:1 to 1:1 in single cell (B). APD (open circle) is displayed versus stimulus number at BCL_2 when BCL was changed from $\mathrm{BCL}_1 = 500$ ms to $\mathrm{BCL}_2 = 170$ ms. Here, $\alpha = 0.1$ (A), $\alpha = 0.6$ (B) and $\tau = 11.4$ s. Dashed lines represent $A_1^{\mathrm{thr}} = \mathrm{BCL}_2 - D_{\min}$ and $A_2^{\mathrm{thr}} = 2\mathrm{BCL}_2 - D_{\min}$.

Fig. 4 : Dynamic responses of single cell at steady state as a function of α when BCL was decreased from BCL_1 to different BCL_2 for $\tau = 11.4$ s (A), $\tau = 260$ ms (B), and $\tau = 200$ ms (C). Behaviors are classified as 1:1 (filled circles or upper right corner regions labeled as 1:1), 2:2 (or alternans) (crosses) and CB.

Fig. 5 : Effect of overpacing in cable. Transition from CB_1 (A) to SCA

(B) and SDA (C, D) and then to CB_2 (E) as BCL was decreased from BCL_1 to $BCL_2 = 220$ ms. Here, $\alpha = 0.175$, $\tau = 11.4$ s and $CV = V_1$. Transition (F) from CB_1 to SDA and then to 1:1 response as BCL was decreased from BCL_1 to $BCL_2 = 190$ ms. Here $\alpha = 0.425$, $\tau = 11.4$ s and $CV = V_1$.

Fig. 6 : Stable (A) and unstable (B) SDA nodal behaviors. APD of selective beats are displayed versus cable length when BCL was decreased from BCL_1 to $BCL_2 = 240$ ms (A) and $BCL_2 = 210$ ms (B), $\alpha = 0.175$ (A), $\alpha = 0.3$ (B), $\tau = 11.4$ s and $CV = V_1$ (steep CV restitution).

Fig. 7 : X_{ss} and t_{ss} as a function of α for stable nodes when BCL was decreased from BCL_1 to $BCL_2 = 130$ ms, $\tau = 200$ ms and $CV = V_1$ (steep CV restitution).

Fig. 8 : Dynamical responses of the cable at steady state as a function of α when BCL was changed from BCL_1 to different BCL_2 for $CV = V_2$, $\tau = 11.4$ s (A), $\tau = 260$ ms (B) and $\tau = 200$ ms (C); $CV = V_1$, $\tau = 11.4$ s (D), $\tau = 260$ ms (E), $\tau = 200$ ms (F). Behaviors were classified as 1:1 response (filled circle or upper right corner regions labeled as 1:1), SDA (cross), SCA (square), CB_1, CB_2 (diamond), transition from CB_1 to CB_2 (star, $CB_1 \rightarrow CB_2$) and unstable nodes (plus, unstable).

458 **9. Figures**

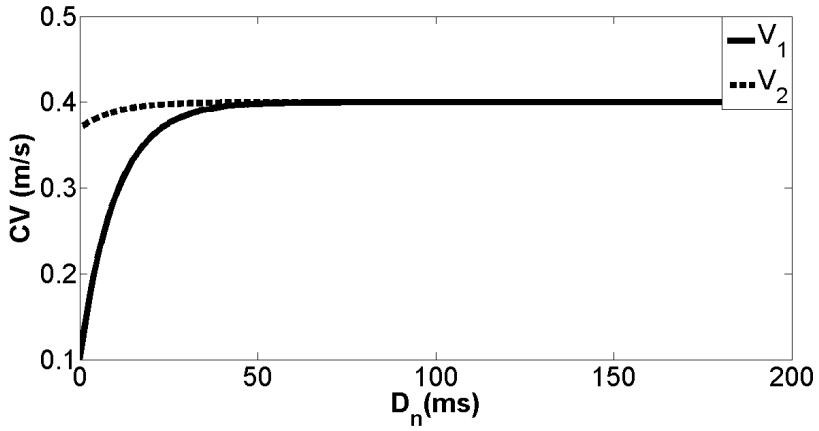

Figure 1

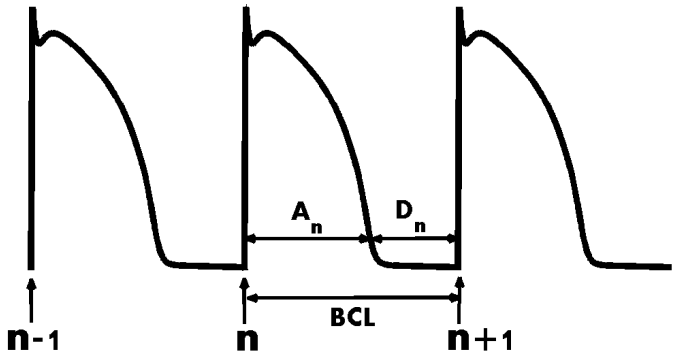
A_n
D_n
BCL
n-1
n
n+1

A

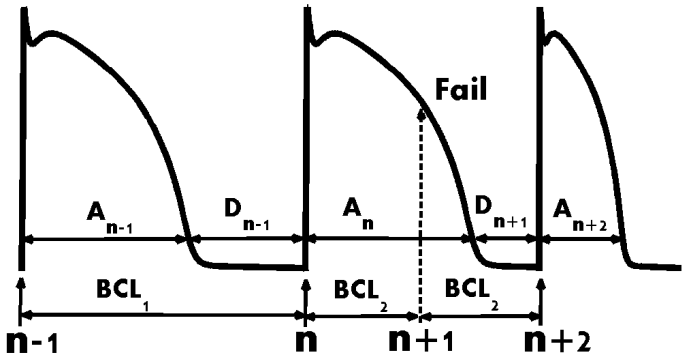
Fail
A_n-1
D_n-1
A_n
D_n+1
A_n+2
BCL_1
BCL_2
BCL_2
n-1
n
n+1
n+2

B

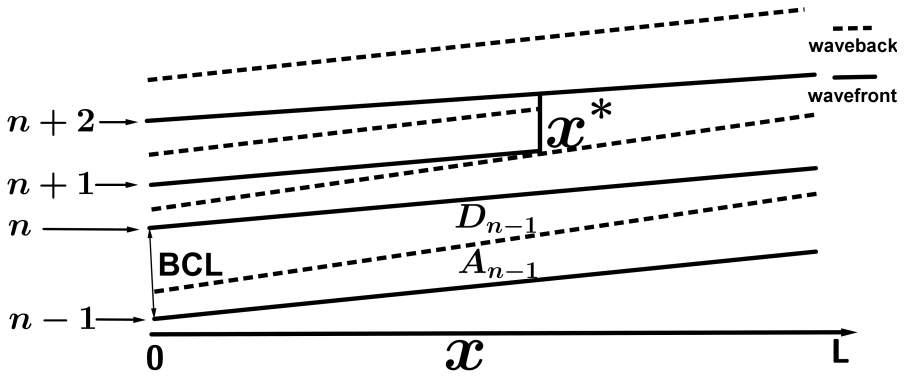
waveback
wavefront
n + 2
n + 1
n
n − 1
x*
D_n−1
A_n−1
BCL
0
x
L

C

Figure 2

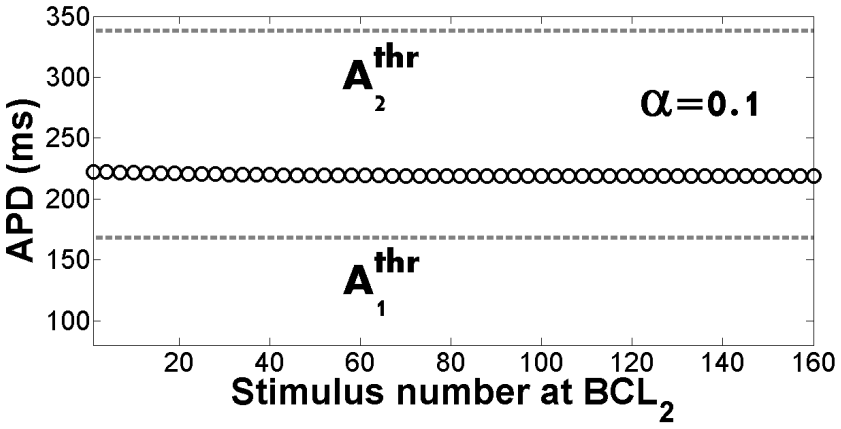
350
300
250
200
150
100
APD (ms)
A_2^{thr}
A_1^{thr}
α=0.1
20
40
60
80
100
120
140
160
Stimulus number at BCL_2

A

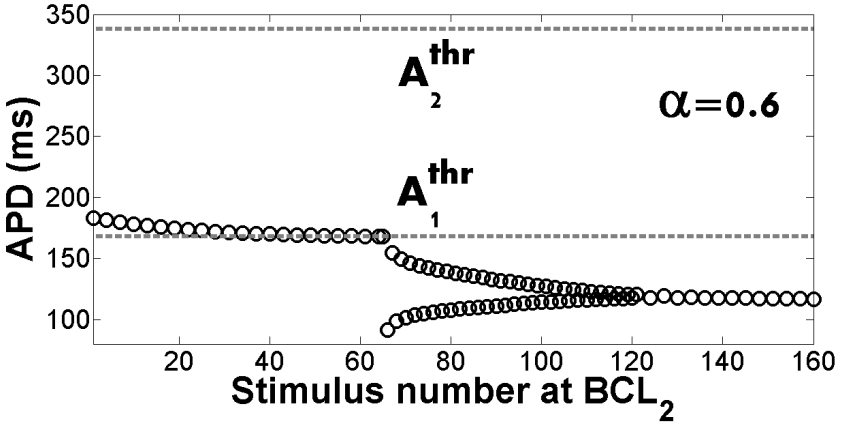
350
300
250
200
150
100
APD (ms)
A_2^{thr}
A_1^{thr}
α=0.6
20
40
60
80
100
120
140
160
Stimulus number at BCL_2

B

Figure 3

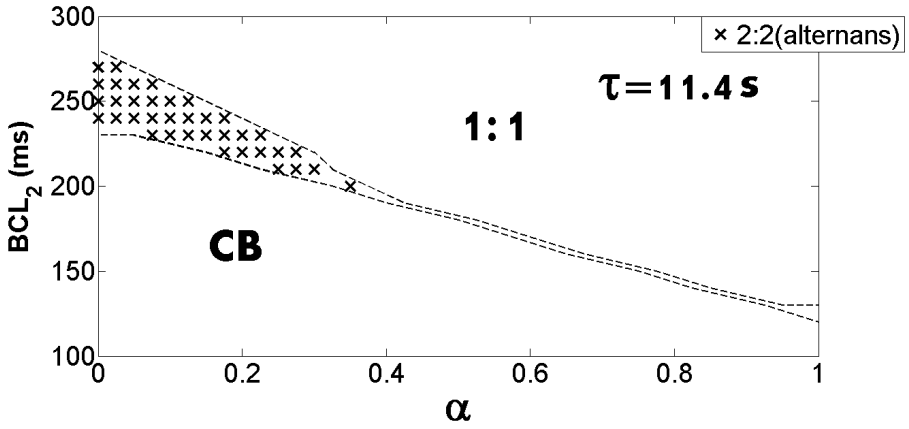
× 2:2(alternans)
τ=11.4 s
1:1
CB
BCL2 (ms)
α
300
250
200
150
100
0
0.2
0.4
0.6
0.8
1

A

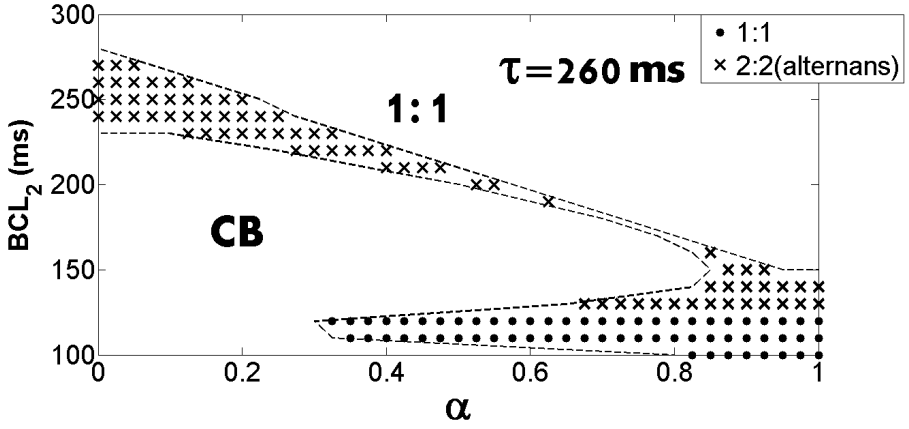
• 1:1
× 2:2(alternans)
τ=260 ms
1:1
CB
BCL2 (ms)
α
300
250
200
150
100
0
0.2
0.4
0.6
0.8
1

B

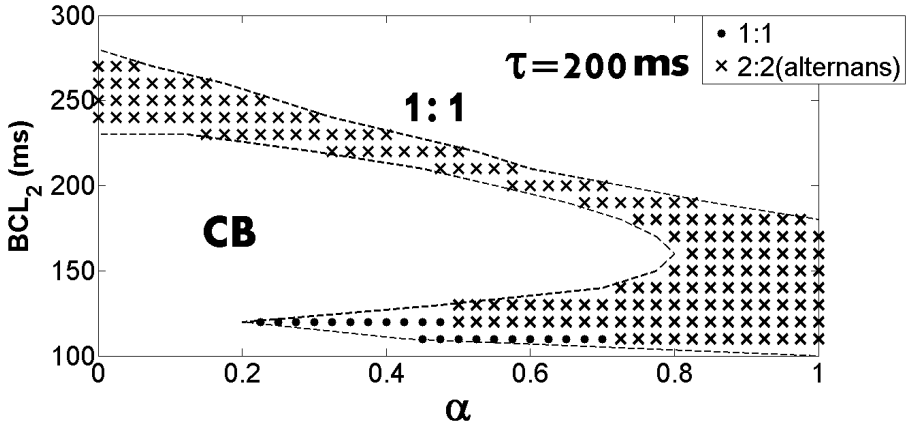
• 1:1
× 2:2(alternans)
τ=200 ms
1:1
CB
BCL2 (ms)
α
300
250
200
150
100
0
0.2
0.4
0.6
0.8
1

C

Figure 4

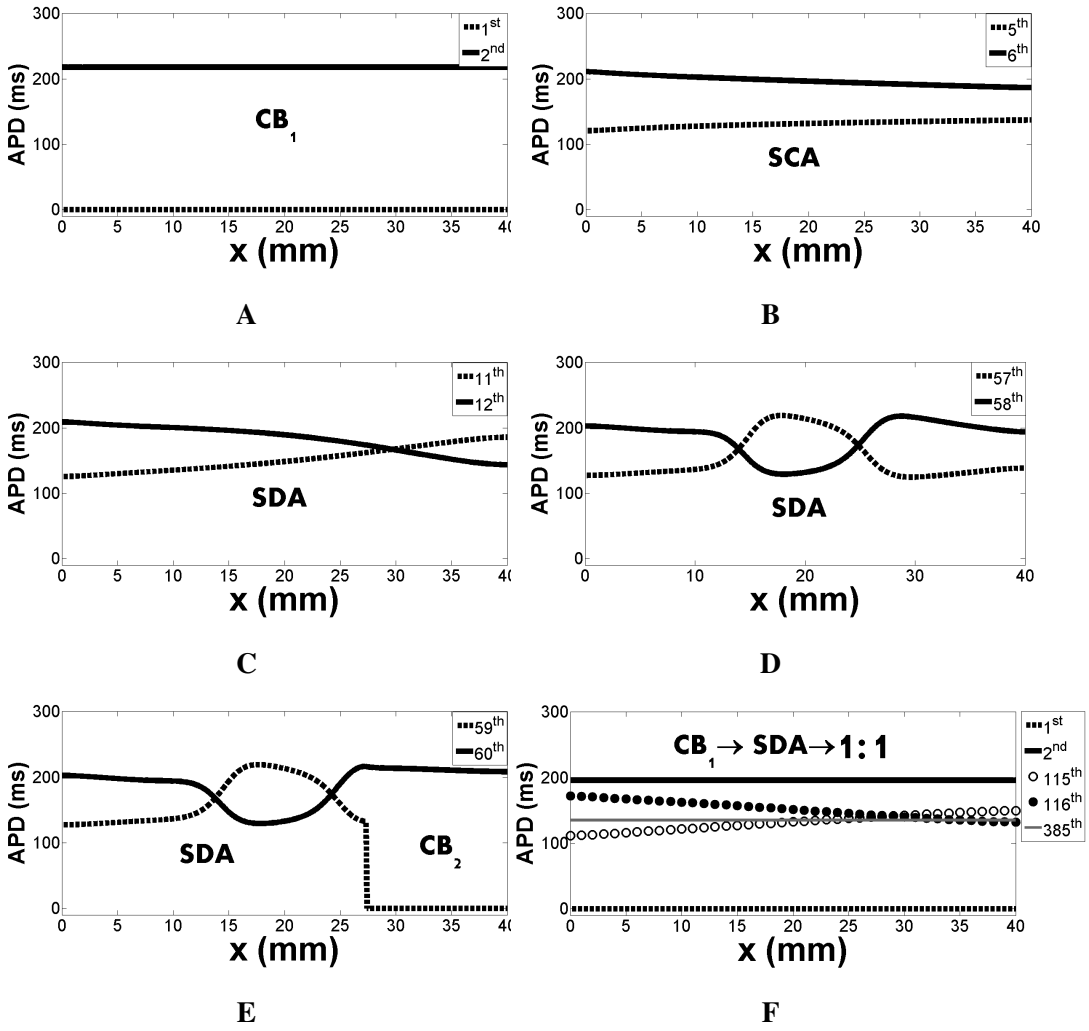
APD (ms)
x (mm)
1st
2nd
CB1
A
5th
6th
SCA
B
11th
12th
SDA
C
57th
58th
SDA
D
59th
60th
SDA
CB2
E
CB1 → SDA→1:1
1st
2nd
115th
116th
385th
F

Figure 5

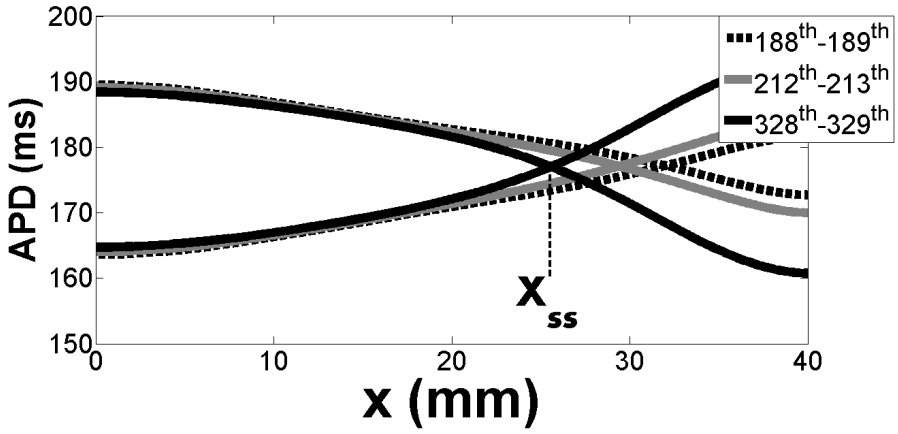
200
190
180
170
160
150
APD (ms)
0
10
20
30
40
x (mm)
188th-189th
212th-213th
328th-329th
x ss

A

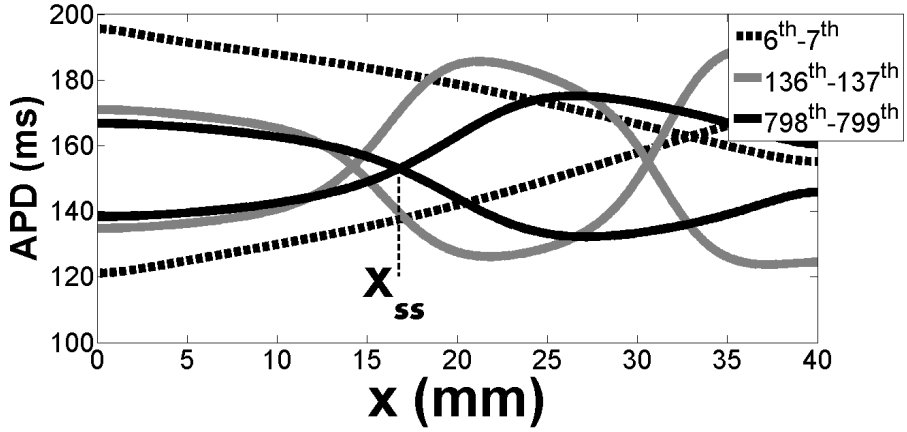
200
180
160
140
120
100
APD (ms)
0
5
10
15
20
25
30
35
40
x (mm)
6th-7th
136th-137th
798th-799th
x ss

B

Figure 6

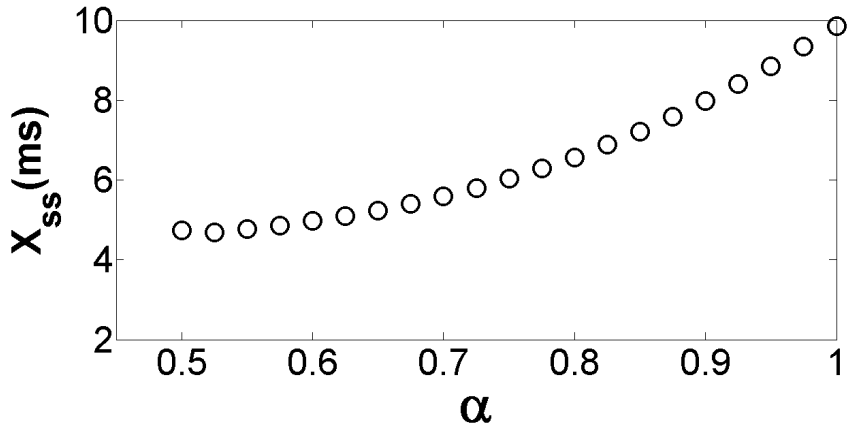
10
8
6
4
2
X_{ss}(ms)
0.5
0.6
0.7
0.8
0.9
1
α

A

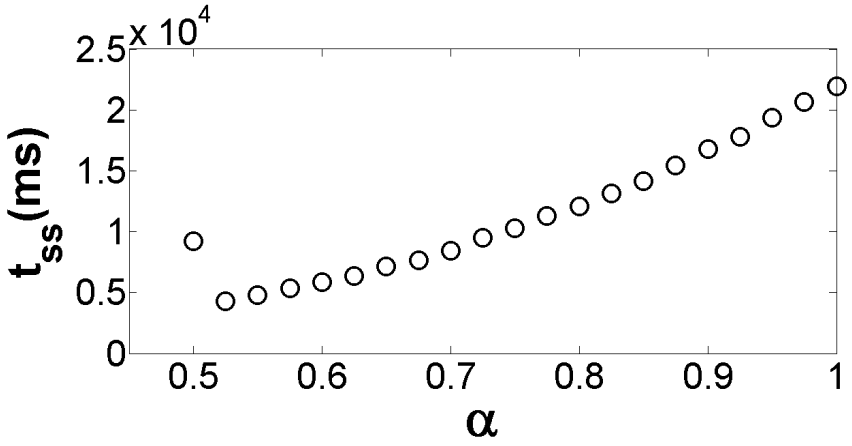
x 10^4
2.5
2
1.5
1
0.5
0
t_{ss}(ms)
0.5
0.6
0.7
0.8
0.9
1
α

B

Figure 7

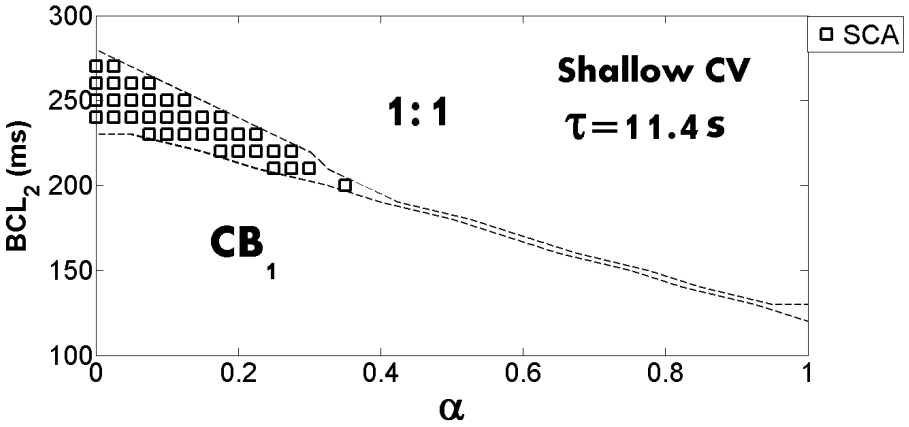
SCA
Shallow CV
τ=11.4 s
1:1
CB1
BCL2 (ms)
α

A

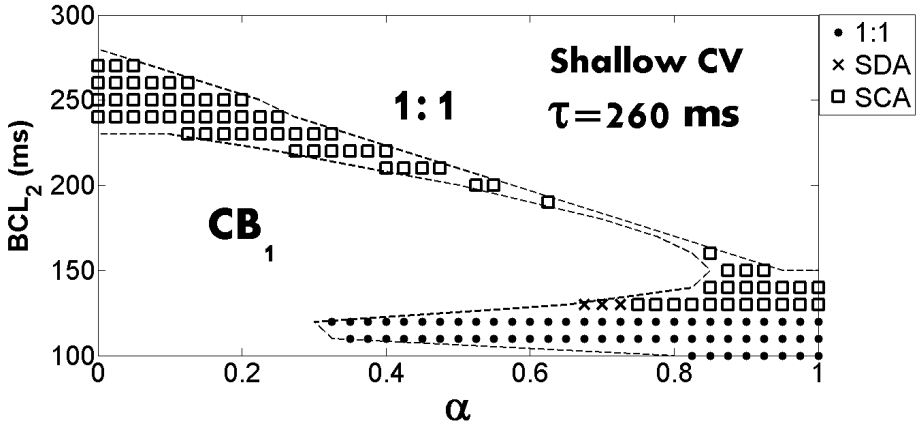
1:1
SDA
SCA
Shallow CV
τ=260 ms
1:1
CB1
BCL2 (ms)
α

B

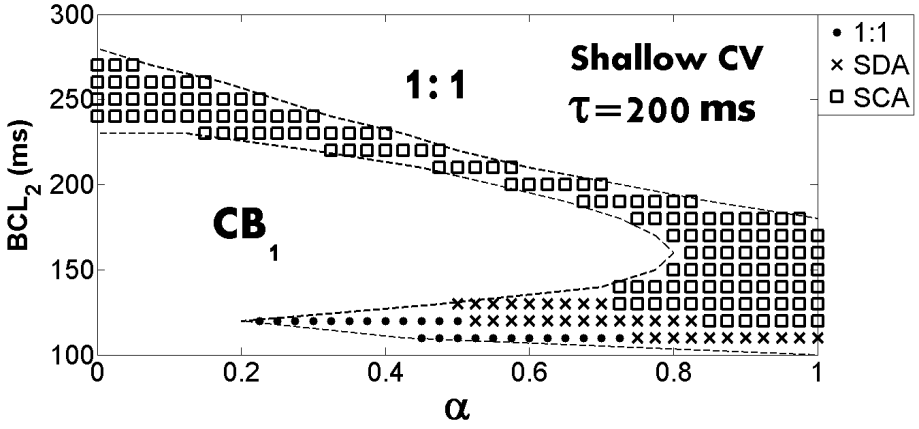
1:1
SDA
SCA
Shallow CV
τ=200 ms
1:1
CB1
BCL2 (ms)
α

C

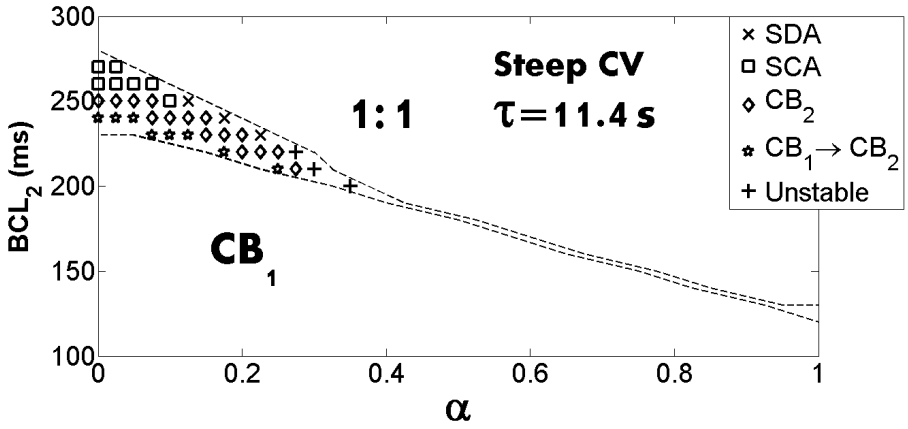
Steep CV
1:1
τ=11.4 s
CB1
× SDA
□ SCA
◇ CB2
✲ CB1→ CB2
+ Unstable
BCL2 (ms)
α

D

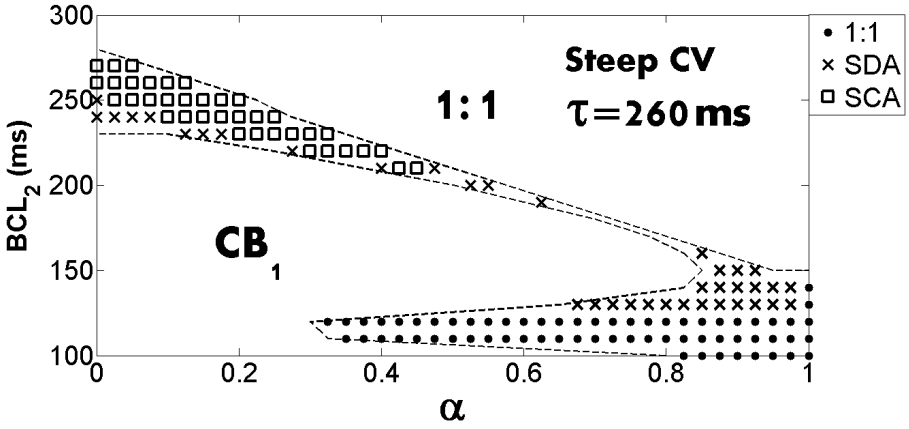
Steep CV
1:1
τ=260 ms
CB1
• 1:1
× SDA
□ SCA
BCL2 (ms)
α

E

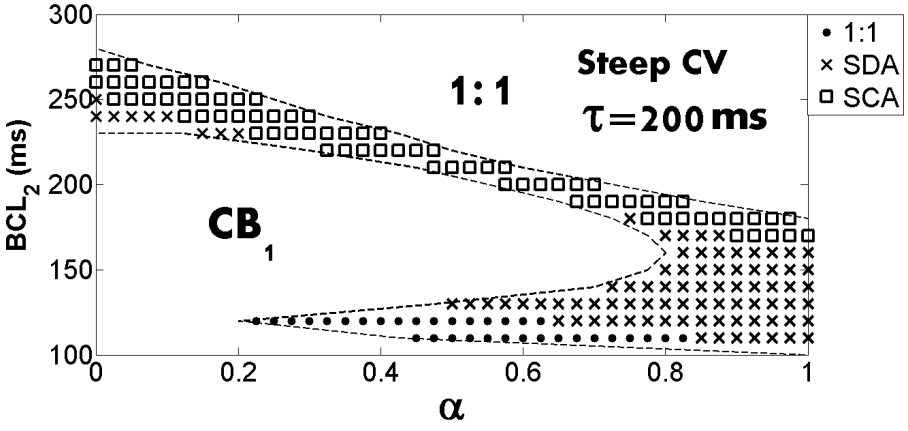
Steep CV
1:1
τ=200 ms
CB1
• 1:1
× SDA
□ SCA
BCL2 (ms)
α

F

Figure 8

10. Tables

Table 1: Parameters Abbreviations

Parameter	Meaning	Value
$D_{\min}$	minimum DI for which action potential can be initiated.	2 ms
BCL_1	Initial BCL in the pacing protocol.	500 ms
BCL_2	Second BCL in the jump pacing protocol.	100 ms to 300 ms
X_{ss}	Steady state positions of nodes in the cable.	
t_{ss}	Time to steady state of the nodes in the cable.	
A_1^{thr}	Threshold for APD without overpacing.	$A_1^{\mathrm{thr}} = \mathrm{BCL}_2 - D_{\min}$.
A_2^{thr}	Threshold for APD including overpacing.	$A_2^{\mathrm{thr}} = 2\mathrm{BCL}_2 - D_{\min}$.
CB	Conduction block in the single cell. or cable.	
CB_1	Type I conduction block in the cable. (Block occurs at $x = 0$).	
CB_2	Type II conduction block in the cable. (Block occurs at $x \neq 0$).	
V_1	Steep CV restitution curve.	$V_1 = 0.4 - 0.3\exp(-\mathrm{DI}/10)$.
V_2	Shallow CV restitution curve.	$V_2 = 0.4 - 0.03\exp(-\mathrm{DI}/10)$.
x	Position in the cable.	
L	Length of the cable.	4 cm